Metall. Res. Technol. **118**, 204 (2021)

https://doi.org/10.1051/metal/2021006

Metallurgical Research & Technology

Available online at:
www.metallurgical-research.org

Regular Article

Identification of crystal plasticity parameters for a non-irradiated and irradiated A508 bainite steel

Can-Ngon Nguyen[1,*], Georges Cailletaud[2], Fabrice Barbe[3], Bernard Marini[4], Duy-Duan Nguyen[1,**], and Huy-Thien Phan[1]

[1] Department of Civil Engineering, Vinh University, 182 Le Duan, Vinh 461010, Vietnam
[2] Mines Paristech, Centre des Matériaux, CNRS UMR 7633, 91003 Évry, France
[3] Normandie Univ, UNIROUEN, INSA Rouen, CNRS, Groupe de Physique des Matériaux, 76000 Rouen, France
[4] Université Paris-Saclay, CEA, SRMA, 91191 Gif-sur-Yvette, France

Received: 9 August 2020 / Accepted: 26 January 2021

Abstract. This paper presents the identification of dislocation-density-based crystal plasticity parameters for a A508 Cl3 bainite steel in non-irradiated and irradiated states and at different temperatures. The representative volume element for the identification process is a cube containing 1000 steel grains represented by a Voronoi mosaic discretized by finite elements. The grains are assigned crystallographic orientations corresponding to an isotropic texture. The crystal constitutive model is based on a plastic flow law, a hardening law, and a law of evolution of dislocation densities. Modeling parameters are determined by a two-step calculation with two different crystal structures: (1) using a simple structure with 343 identical grains to identify 7 parameters, (2) using a Voronoi tessellation of 1000 grains to refine the parameters. Thereafter, the calculated stress-strain curves are compared with experimental stress-strain curves. The results show that the simulated stress-strain curves are in good agreement with those of experiments, highlighting the reliability of the proposed procedure to account for the significant effects of irradiation and temperature.

Keywords: parameters identification / crystal plasticity / microstructure / A508 bainite steel / irradiation

1 Introduction

The A508 Cl3 steel is a low alloy steel used to manufacture heavy components of the primary circuit of nuclear Pressurized Water Reactor (PWR). This steel has a bainitic microstructure [1] and is used in particular for the vessel, which contains the fuel elements of many nuclear power plants worldwide. For nuclear power plants, safety is always the most important issue, so the integrity of the vessel is paramount. The key to understanding this problem is the evaluation of the risk of brittle fracture under hypothetical accidental conditions. So, to evaluate this risk, it is essential to understand formation, distribution, development of micro-cracks, which can be at the origin of the brittle fracture of the component. Moreover, the detailed information about the modifications of stress and strain distributions in each steel grain when exposed to radiation is very important and the microstructure is the key of these evolutions [2,3]. In this study, we derive this information by means of a physics-based model which includes the following elements:

- explicit description of the evolution of the dislocations population;
- microstructures with a sufficient size in terms of number of grains to be a representative volume at the macroscale and a description of the characteristic shape of the steel grains at two degrees of accuracy with respect to real microstructures: either a simplified microstructure with monodisperse grains, or a complex microstructure as given by a Voronoi tessellation and hence with random morphologies and size distribution of grains;
- a discretization of the microstructure at two degrees of refinement: a single element for each grain in the simplified microstructure or, for the complex microstructure, an intragranular discretization of the grains with grain boundaries conforming to elements boundaries, which enables to account for the local intragranular interactions taking place between grains;
- a model written in a large deformation framework [4–7].

* e-mail: canngon.ng@gmail.com
** e-mail: duyduankxd@vinhuni.edu.vn

In the present paper, the aim is to describe the stress-strain behavior of the A508 Cl3 steel before and after a significant neutron irradiation dose. To this purpose, a set of 15 required parameters need to be identified. The numerical simulation results are compared with those of experimental tests at different temperatures and irradiation states.

2 Constitutive model

The model is built on the basis of the dislocation-density-based model presented in Libert et al. [8]. This model is based on three evolution laws: (1) a temperature dependent plastic flow law developed by Louchet [9] and generalized by Kocks [10], (2) a hardening law developed by Rauch [11], and (3) dislocation density evolution developed by Tabourot [12]. The choice of this model is motivated by the need to describe the constitutive behavior at temperatures above and below the transition temperature, characterized by a transition in the involved deformation mechanisms, viz. athermal or thermally activated mechanisms, double kink formation, preferential activation of the slip system families <1 1 0> {1 1 1} or <1 1 2> {1 1 1}. This model enables to account both for short-range barriers due to obstacles or lattice friction and long-range effects such as the elastic stresses induced by forest dislocations. The equations of the model and the physical meaning of each parameter are presented in the following.

2.1 Plastic flow law

The plastic flow law, as expressed in equation (1), provides the evolution of the slip rate $\dot{\gamma}^s$ on a system s according to the temperature T and to the reference slip rate $\dot{\gamma}_0$ in the temperature-independent regime.

$$\begin{aligned}\dot{\gamma}^s &= \dot{\gamma}_0 \exp\left[-\frac{\Delta G(\tau_{eff})}{k_b T}\right] sign(\tau_s) \\ &= \dot{\gamma}_0 \exp\left[-\frac{\Delta G_0}{k_b T}\left(1-\left(\frac{\tau_{eff}}{\tau_R}\right)^p\right)^q\right] sign(\tau_s)\end{aligned} \quad (1)$$

where k_B is the Boltmann constant, $\Delta G(\tau_{eff})$ is the activation energy for double kink: it is the energetic barrier to be overcome for a dislocation to transfer from a Peierls valley to another. As proposed by Kocks et al. [10], it depends on the effective stress τ_{eff}, which is the applied shear stress subtracted by the athermal shear stress due to forest dislocations and precipitates. τ_{eff} is mostly related to lattice friction, which corresponds to short-range interactions, whereas forest dislocations are at the origin of long-range interactions. τ_R is the shear stress required to generate a double kink at $T = 0\,\mathrm{K}$. ΔG_0 is the nucleation energy of a double kink without the contribution of the thermal activation. p, q are the parameters enabling to shape the energy of the Peierls barriers.

2.2 Hardening law

The shear stress τ^s necessary to activate slip on the system s is the sum of three contributions accounting for short and long range interactions related to lattice friction (via τ_{eff}), forest dislocations (via τ_{int}), precipitates and boundaries (via τ_0):

$$\tau^s = \tau_{eff} + \tau_0 + \tau_{int} \quad (2)$$

where τ_{int} is defined, after Rauch [11], by equation (3). It represents long-range interactions due to forest dislocations which density is given by ρ.

$$\tau_{int} = \frac{(\alpha\mu b)^2 \rho}{\tau^s - \tau_0} \quad (3)$$

μ is the elastic shear modulus and b is the Burgers vector norm. Tabourot [12] has proposed to replace the overall effect of dislocation interactions, handled by α, by an explicit representation of the slip system interactions by means of the interaction matrix α^{su} introduced by Franciosi [13]. This has led to equation to define τ_{int}.

$$\tau_{int} = \frac{(\mu b)^2 \sum_u \alpha^{su} \rho^u}{\tau^s - \tau_0} \quad (4)$$

where ρ^u is the dislocation density on the slip system u. τ_0 is the hardening contribution, which has been introduced by Rauch [11] in order to account for the presence of precipitates and obstacles, which are specific to steels as compared to pure iron, because of the alloying elements. As expressed in equation (5), τ_0 depends on the considered slip system family, after Libert [14] and Libert et al. [8], it is proposed to distinguish the sensitivity of the slip systems families {110} and {112} to temperature by means of the function $f(T)$ which has been determined from experimental analyses.

$$\tau_0^{110} = \tau_0 \quad ; \quad \tau_0^{112} = \tau_0 + f(T) \quad (5)$$

2.3 Dislocation density evolution

The dislocation density rate $\dot{\rho}^s$, as expressed in equation (6), is taken from the model of Tabourot [12], which was developed for bcc metals at temperatures above the transition temperature. The extension of this law to low temperatures is discussed hereafter.

$$\dot{\rho}^s = \frac{|\dot{\gamma}^s|}{b}\left(\frac{1}{D_{grain}} + \frac{\sqrt{\sum_{s\neq u}\rho^u}}{K(T)} - g_c(T)\rho^s\right) \quad (6)$$

The rate of production of dislocations on a system s is proportional to (i) the slip rate $\dot{\gamma}^s$ and (ii) three terms describing the state of the microstructure. The first two terms define the capacity of dislocation multiplication according to the mean free path of dislocations which itself depends on microstructure characteristic size, namely the size of a bainite lath D_{grain}, and on the total number of dislocations being present the second positive term. The third term corresponds to the rate of dislocation

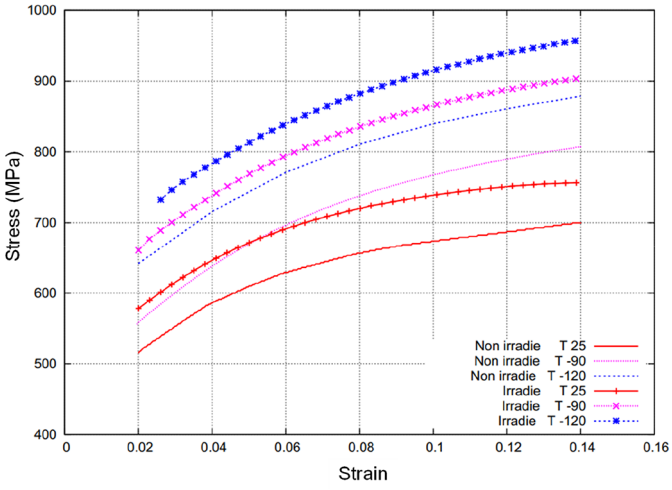

Fig. 1. The reference stress-strain curves of simple tensile tests of non-irradiated and irradiated material at different temperatures [15].

annihilation and is thus assigned a negative sign. The temperature dependence is first introduced with the parameter $K(T)$, which acts on dislocation multiplication: the larger $K(T)$ the smaller the capacity to have dislocation nucleation. $K(T)$ is directly given temperature dependent values from the identification process. The second temperature dependence is introduced in the competitive mechanism of dislocation annihilation, which is controlled by the parameter $g_c(T)$: the larger T the larger $g_c(T)$. As for $K(T)$, $g_c(T)$ is directly identified at different temperatures.

3 Context of the identification

3.1 Reference experimental data

The identification is based on reference stress-strain experimental responses as presented in Figure 1. They correspond to an irradiated and a non-irradiated state and for each state of irradiation, different temperatures are considered. The experiments were performed with cylindrical samples of 5 mm diameter, 30 mm length, imposed strain rate of $0.5 \times 10^{-4}\,\mathrm{s}^{-1}$ until reaching a deformation of 14%. These data were provided by CEA [15].

3.2 Predefined parameters

In his work, Libert [14] has identified different parameters from the stress-strain behavior of the considered steel. Table 1 provides the values of these parameters. A first class corresponds to parameters which are representative of the considered steel: the three components of elastic stiffness ($C11$, $C12$, and $C44$), the norm of the Burgers vector (b), the slip rate at the thermally independent regime ($\dot{\gamma}_0$), and the coefficients of the slip systems interaction matrix (α^{su}). A second class is deduced from direct observations of the microstructure: the average size of bainite laths (D_{grain}) and the initial dislocation density (ρ_o). The function $f(T)$ describing the dependence of the reference resolved shear stress (τ_0) to temperature (Eq. (5)) was also provided.

These parameters, as given in Table 1, are fixed in the identification procedure since they are representative of the considered steel whatever its state of irradiation. There then remain 7 parameters have to identify:

- The activation energy for double kink (ΔG_0);
- The absolute shear stress to move dislocation at $\mathrm{T} = 0\,\mathrm{K}$ (τ_R);
- The reference resolved shear stress taking into account the role of carbon compounds, precipitates and obstacles at grain boundaries and other crystal defects (τ_0);
- Parameters defining the shape of the activation energy caused by obstacles (p, q);
- The temperature dependent coefficient characterizing the mean free path dependence of dislocation multiplication to the dislocation density ($K(T)$);
- The temperature dependent coefficient characterizing the term of dislocation annihilation rate ($g_c(T)$).

3.3 Preliminary analysis

As detailed in [16], considering the different equations of the constitutive model, several preliminary conclusions on the respective roles of parameters can be drawn. First, considering equation (1), for a given slip rate $\dot{\gamma}^s$ and a given temperature T, the effective shear stress τ_{eff} depends on 4 undetermined parameters:ΔG_0, τ_R, p, q. Hence, these parameters may affect not only the yield stress but also the rate of hardening (the shape of the stress-strain curve in the hardening regime). Considering equation (4), τ_0 can be considered to affect the yield stress. Considering equation (6), it is deduced that the two remaining undetermined parameters $K(T)$, $g_c(T)$ may only affect the relation of dislocation density rate to slip rate, i.e. the shape of the curve in the hardening regime.

The dependence of the stress-strain curves on temperature will be handled by τ_0 on one side (as described in Eq. (5)), which will act on the yield stress, and on $K(T)$, $g_c(T)$ on the other side, which will act on the hardening rate. Finally, in order to respect the physical meanings of the parameters, considering how irradiation affect the tensile properties and the respective aforementioned roles of parameters, the dependence of the constitutive behavior to the state of irradiation will be accounted for through the parameters ΔG_0 and τ_0.

3.4 Bounds of parameters

The analyses presented in the work of Groh and Conte [17] enable to fix bounds for the parameters p, q, ΔG and τ_R as presented in Table 2. This directly defines the domain within which these parameters will be varied during the identification procedure.

Table 1. Value of the initial parameters for A508 Cl3 steel after [14].

$C11$ (GPa)	$C12$ (GPa)	$C44$ (GPa)	$\dot{\gamma}_0(\mathrm{s}^{-1})$	D_{grain} (μm)	b(m)	α^{su}	$\rho_0(\mathrm{m}^{-2})$
275,2	112.4	81.4	10^6	2.5	2.51×10^{-10}	0.25	10^{14}
24 slip systems, two families {110} and {112}							
$\tau_0^{110} = \tau_0$							
$\tau_0^{112} = \tau_0$			if $T > 206$ K				
$\tau_0^{112} = \tau_0 + 73.6 - 0.357\,T$			if $T \leq 206K$				

Table 2. Bounds of parameters after [17].

P	q	ΔG(eV)	τ_R(MPa)
0.25	0.75	0.70	350
0.75	1.5	1.25	500

4 Procedure for identifying material parameters

The bainite steel has a complex hierarchical microstructure: primary austenite grains have transformed into bainite packets during cooling-controlled phase transformation and themselves are divided into laths. Whereas the crystallographic misorientation between laths of a same bainite packet remains small (below 5°), bainite packets have crystallographic orientations which differ strongly from a packet to the other and which are all related to the crystallographic orientation of the primary austenite grain they belong to [5]. The orientation relationships can be described according to the Kurdjumov–Sachs (KS) or Nishiyama–Wassermann (NW) rules [18].

Due to the complexity of the microstructure and the large number of parameters to manipulate, the identification process of material parameters is divided into two steps: (1) The first step is a rough identification of the parameters from a simplified representation of the microstructure which enables rapid simulations; (2) The second step is a refinement of the pre-identified parameters from a microstructure accounting for the main microstructural characteristics of the bainitic steel.

The microstructures are generated from the Neper software [19,20]. Simulations have been performed with the parallel solver of the Z-set finite element software [21]. The full and detailed procedure of microstructure generation, meshing, assignation of material properties and crystallographic orientations, post-processing, and examples of application of this procedure on a wide range of microstructures can be found in [22–27].

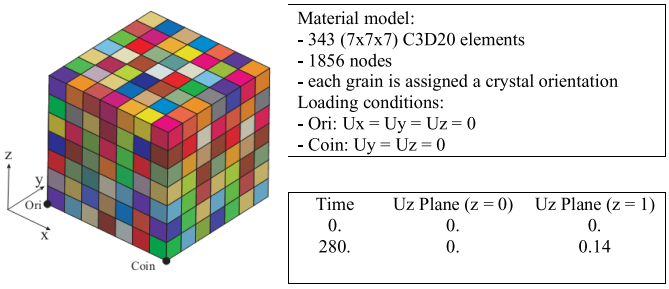

Fig. 2. Simplified RVE for the first step of the identification. Each finite element represents a crystal.

4.1 First step: simplified microstructure

For the first step of parameters identification, a simple polycrystalline Representative Volume Element (RVE) is used. It corresponds to a cube regularly meshed into identical 20-node-brick elements with quadratic integration. Each element represents a grain (or a crystal). Numerous studies [22–24] pointed out that, for an isotropic polycrystal of a bcc or fcc material, the number of grains in the RVE should be of the order of 200 to provide effective elastoplastic properties of the polycrystal. It was further shown that assigning each single crystal to a single element of the mapped mesh enables to obtain efficiently a first-degree estimation of these effective properties. The RVE selected for this preliminary determination is constituted of $7 \times 7 \times 7$ crystals (i.e. 343 elements). It is subjected to a simple tension with displacements imposed at the rate of the experiments, as shown in Figure 2.

4.2 Second step: high resolution microstructure

The second step of the identification procedure consists in refining the parameters obtained on the first step by considering a more realistic RVE in terms of (i) the considered number of crystals, (ii) the morphologies of the crystals and (iii) the finite element discretization of each crystal. The RVE now contains 1000 crystals which are defined by the polyhedra of a Voronoi tessellation. Modeling the microstructure of a polycrystal by a Voronoi

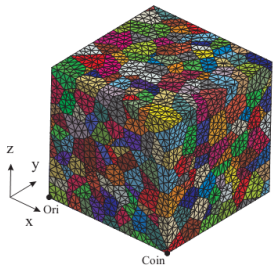

Material model:
- 74 442 C3D10 elements
- 104 092 nodes
- each grain is assigned a crystal orientation

Load conditions:
- Ori U1 0.; U2 0.; U3 0.
- Coin U2 0.; U3 0.

Times	U3 plane (z = 0)	U3 plane (z = 1)
0.	0.	0.
280.	0.	0.14

Fig. 3. High resolution RVE for the second step of the identification. Each color represents a crystal, which itself is discretized into several tetrahedral elements.

mosaic is a widely accepted solution when considering the random nature of grain morphologies in a polycrystal [25,28,29]. As seen on Figure 3, each crystal is discretized into tens of tetrahedral elements (10-node-tetrahedra with quadratic integration) and grain boundaries conform to finite element boundaries. This corresponds to the adopted strategy for the prediction of micro-fractures arising at the local scale of the grains [27].

4.3 Crystallographic orientations in the high-resolution microstructure

As detailed in [5,6], whereas the crystallographic misorientation between bainite packets of a given primary austenite grain can be large, it is less than 5° between laths of a given packet. This justifies, as in [5], to distinguish bainite packets in the polycrystalline representation and to consider laths of a given packet as having the same crystallographic orientation. Hence, each polyhedron of the high resolution RVE represents a bainite packet.

Yet, the study [5] also indicates that in order to correctly describe the intra- and intergranular elastoplastic interactions, the crystallographic orientations of the bainite packets should respect the orientation relationships with the primary austenite grain they belong to. Two types of relationships can be adopted to this purpose: (1) Kurdjumov–Sachs (KS), which lead to 24 variants, or (2) Nishiyama–Wassermann (NW), which leads to 12 variants [18].

The analyses presented in [5–7] further indicate that a primary austenite grain contains of the order of 20–50 bainite packets. Different solutions for the assignment of the 1000 bainite packets to primary austenite grains are then possible. In order to analyze the effect of the number of packets per primary austenite grain on the effective tensile properties of the polycrystal, a preliminary analysis has been made, by considering two configurations: either 20 or 50 primary austenite grains, which respectively corresponds to 50 and 20 bainite packets per primary austenite grains. Each configuration has been tested by using the KS and the NW relationships. This analysis is completed with the case where bainite packets are assigned random crystallographic orientations.

The macroscopic stress-strain curves in these five configurations are shown in Figure 4. The results show that there is no effect of the crystal orientation assignment

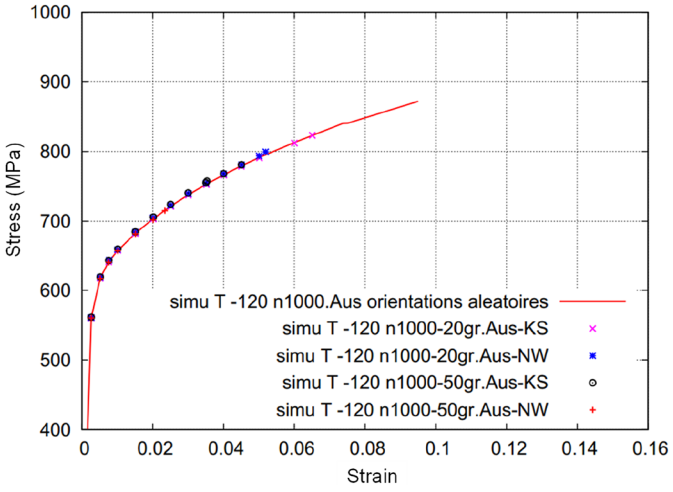

Fig. 4. Macroscopic stress-strain tensile curves obtained from the high resolution RVE with different crystal orientation assignments: 20 or 50 primary austenite grains (and thus 50 or 20 bainite packets par primary grain); KS or NW relationships, or random orientations.

procedure on the effective properties of the polycrystal. This further confirms that the number of crystals is large enough for providing the effective isotropic properties of the bainite steel. Following these analyses, the configuration of randomly set crystallographic orientations has been selected for conducting the identification at the second step.

Since the reference tensile strain-stress curves are established for strains up to 14% and since the final use of the polycrystalline model deals with that range of strains, the constitutive model has been implemented in the large deformation framework [16], and all simulations for the identification have been performed within this framework. Each simulation with the simplified RVE takes about 4 h. By means of several iterations, a first estimation of the 7 considered parameters could be obtained within few days. Each simulation with the high resolution RVE has been parallelized onto a cluster of 8 computers and took about 110 h. In order to reduce the number of identification iterations for these long run and computationally consuming tensile test simulations of the second step, only the parameters K and gc were to be adjusted with the High resolution RVE.

5 Results and discussion

The stress-strain curves obtained with the identified set of parameters are shown in Figures 5 and 6. The values of the parameters are presented in Tables 3 and 4. Figures 5 and 6 show the very good agreement which could be obtained for both states of irradiation and for all the temperatures. Conforming to the analyses of the role of the parameters presented in Section 3.3, the differentiation between the irradiated and non-irradiated states is set from the parameters ΔG and τ_0, whereas the effect of temperature is produced by setting temperature-dependent values of the parameters K and g_c. ΔG is the activation energy and τ_0

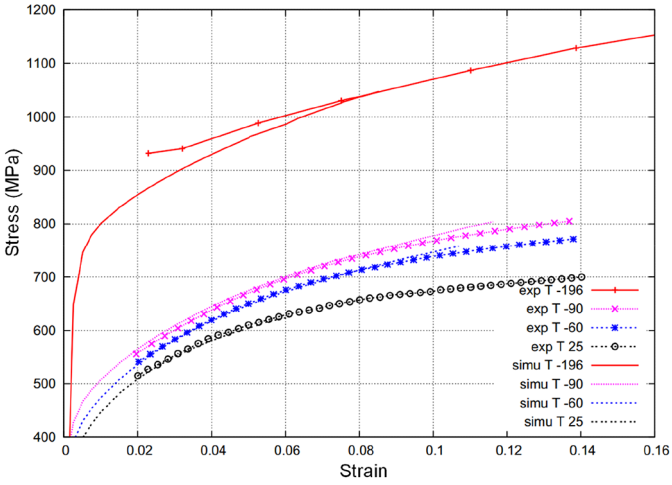

Fig. 5. Simulation and experimental tensile stress-strain curves for the non-irradiated state.

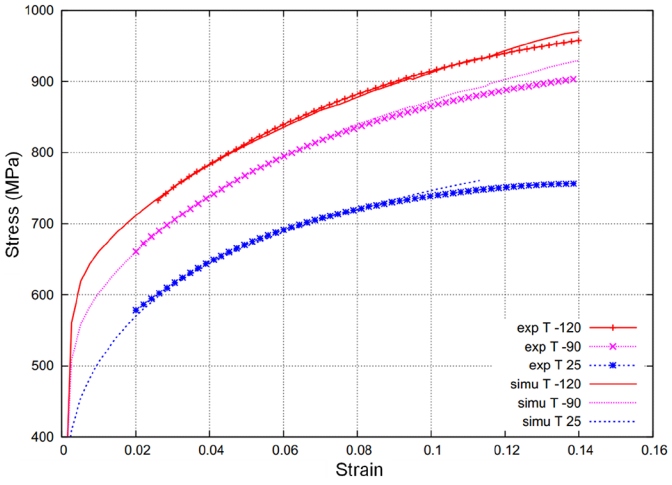

Fig. 6. Simulation and experimental tensile stress-strain curves for the irradiated state.

Table 3. Parameters for non-irradiated material.

Common parameters		Parameters for each temperature					
ΔG	0.749 eV		−196 °C	−90 °C	−60 °C	25 °C	
τ_R	498 MPa	K	120	40	23	12	343 Cubes
τ_0	40.82 MPa	g_{cb}	11,5	26.5	41	87	
p	0.35						
q	1.21	K	75	30	20	11	1000 Voronoi
		g_{cb}	10	25	36.5	77	

takes into account the role of carbon compounds, precipitates and grain boundaries which hinder dislocations glides. The variation of these values according to the state of irradiation can be related to the physical mechanism occurring at the atomic scale: when exposed to neutron radiation, a chain reaction occurs in the crystal lattice creating a cascade of displacements of the iron atoms. This mechanism leads to void defects in the crystal lattice which promote the segregation of compounds and the weakening of grain boundaries. Crystalline defects also promote precipitation at the origin of clusters of defects which hinder the glides of dislocations [30–33]. These physical mechanisms result prominently in an increase on the effective yield stress from the non-irradiated to the irradiated states, which is to be related to the increases of both ΔG and τ_0 as seen in Tables 3 and 4.

As explained in Section 3.3, K and g_{cb} are two parameters affecting the shape of the tensile curve in the tensile regime, and temperature can be observed to affect the hardening response under tension in the experiments, with levels of influence which are only slightly dependent on the irradiation state. This justifies setting the same values for non-irradiated and irradiated states and to have these parameters only depending on temperature. Conforming to the definitions of these parameters in the dislocation-density evolution law (see Sect. 2.3), the identified values of K decrease as T increases whereas g_{cb} increases.

6 Conclusions

This article deals with the elastoplastic constitutive behavior of a bainitic steel used in nuclear reactors. Its conditions of service impose to control the evolution of its properties according to both its irradiation state and the temperature it is exposed to on a range of 200 °C which includes the ductile-fragile transition temperature. Considering the safety-related challenges of nuclear industry on a very long run, many efforts have been made to predict the constitutive elastoplastic behavior of this steel and by extension its fracture probabilities, focusing especially on the rare events. This has motivated the development of constitutive models accounting for the hierarchized microstructure of the steel, from the presence of precipitates at the origin of micro-fractures, to the effective macroscopic scale of the volume element in continuum mechanics. This article constitutes a contribution to these developments. It focuses on the strategy employed for the identification of the complex

Table 4. Parameters for irradiated material.

Common parameters		Parameters for each temperature				
ΔG	0.955 eV		−120 °C	−90 °C	25 °C	
τ_R	498 MPa	K	105	40	12	343 Cubes
τ_0	54.68 MPa	g_{cb}	14	26.5	87	
p	0.35					
q	1.21	K	65	30	11	1000 Voronoi
		g_{cb}	14	25	77	

dislocation-density based and temperature-dependent crystal plasticity model which is assigned to the bainite packets of the steel. This strategy accounts for the polycrystalline nature of the steel: two levels of accuracy in the microstructural representation of the representative volume element are used, as well as different distributions of the orientation relationships between packets. The comparisons of the reference experimental and simulated tensile curves show that the employed model is able to reproduce the effective macroscopic–elastoplastic behavior of the steel at two irradiation states and at different temperatures ranging from −196 °C to the ambient.

Data availability

All the data supporting the key findings of this paper are presented in the figures and tables of the article. Request for other data will be considered by the authors.

References

1. J. Mathieu, Analyse et modélisation micromécanique du comportement et de la rupture fragile de l'acier 16MND5 : prise en compte des hétérogénéités microstructurales, PhD Thesis, École Nationale Supérieure d'Arts et Métiers, 2006
2. L. Vincent, M. Libert, B. Marini, C. Rey, Towards a modelling of RPV steel brittle fracture using crystal plasticity computations on polycrystalline aggregates, J. Nuc. Mat. **406(1)**, 91–6 (2010)
3. B. Marini, X. Averty, P. Wident, P. Forget, F. Barcelo, Effect of the bainitic and martensitic microstructures on the hardening and embrittlement under neutron irradiation of a reactor pressure vessel steel, J. Nuc. Mat. **465**, 20–7 (2015)
4. J. Mathieu, K. Inal, S. Berveiller, O. Diard, A micromechanical interpretation of the temperature dependence of Beremin model parameters for french RPV steel, J. Nucl. Mat. **406**, 97–112 (2010)
5. N. Osipov, A. Gourgues-Lorenzon, B. Marini, V. Mounoury, F. N'Guyen, G. Cailletaud, FE modelling of bainitic steels using crystal plasticity, Phil. Mag. **88(30)**, 3757–3777 (2008)
6. N. Osipov, Génération et calcul de microstructures bainitiques, approche locale intragranulaire de la rupture, PhD. Thesis, École Nationale Supérieure des Mines de Paris, 2007
7. A. Pineau, B. Tanguy, Advances in cleavage fracture modelling in steels: Micromechanical, numerical and multiscale aspects, Comp. Rend. Phys. **11(3-4)**, 316–325 (2010)
8. M. Libert, C. Rey, L. Vincent, B. Marini, Temperature dependant polycrystal model application to bainitic steel behavior under tri-axial loading in the ductile–brittle transition, Intl. J. Solids Struct. **48(14-15)**, 2196–2208 (2011)
9. F. Louchet, L. Kubin, D. Vesely, In situ deformation of bcc crystals at low temperatures in a high-voltage electron microscope-dislocation mechanisms and strain-rate equation, Phil. Mag. A **39(4)**, 433–454 (1979)
10. U. Kocks, A. Argon, M. Ashby, Thermodynamics and kinetics of slip – Progress in Materials Science, Pergamon Press, Oxford, 1975
11. E. Rauch, Étude l'écrouissage des métaux : aspects microstructuraux et lois de comportement, PhD Thesis, Institut National Polytechnique de Grenoble, 1993
12. L. Tabourot, Loi de comportement élastoviscoplastique du monocristal en grandes transformations, PhD Thesis, Institut National Pomytechnique Grenoble, France, 1992
13. P. Franciosi, Glide mechanisms in bcc crystals: An investigation of the case of α-iron through multislip and latent hardening tests, Acta Met. **31(9)**, 1331–1342 (1983)
14. M. Libert, Études expérimentale et numérique de l'effet des mécanismes de plasticité sur la rupture fragile par clivage dans les aciers faiblement alliés, PhD Thesis, École Centrale Paris, 2007
15. CEA, Internal Report, 2010
16. C.N. Nguyen, Modélisation du comportement en plasticité et à rupture des aciers bainitiques irradiés, PhD Thesis, École Nationale Supérieure des Mines de Paris, 2010
17. P. Groh, R. Conte, Stress relaxation and creep in α-iron filamentary single crystals at low temperature, Acta Met. **19(9)**, 895–902 (1971)
18. P. Kelly, Crystallography of lath martensite in steels, Mat. Trans. **33(3)**, 1519–1530 (1992)
19. Neper: Polycrystal generation and meshing, http//www.neper.info, 2020
20. R. Quey, P. Dawson, F. Barbe, Large-scale 3-D random polycrystals for the finite element method: Generation, meshing and remeshing, Comput. Meth. Appl. Mech. Eng. **200**, 1729–1745 (2014)
21. Z-set – Non-linear material and structure analysis suite, http://zset-software.com/
22. F. Barbe, S. Forest, G. Cailletaud, Polycrystalline plasticity under small strains. Toward finer descriptions of microstructures, in: E. Bouchaud et al., ed., NATO Proceedings on Physical Aspects of Fracture, pp. 191–06, Kluwer Academic Publishers, 2001

23. F. Barbe, L. Decker, D. Jeulin, G. Cailletaud, Intergranular and intragranular behavior of polycrystalline aggregates. Part 1: F.E. model, Int. J. Plast. **17(4)**, 513–536 (2001)
24. O. Diard, S. Leclercq, G. Rousselier, G. Cailletaud, Evaluation of finite element-based analysis of 3D multicrystalline aggregates plasticity: Application to crystal plasticity model identification and the study of stress and strain fields near grain boundaries, Int. J. Plast. **21(4)**, 691–722 (2005)
25. F. Barbe, L. Decker, D. Jeulin, G. Cailletaud, Intergranular and intragranular behavior of polycrystalline aggregates, Part 2: Results. Int. J. Plast. **17(4)**, 537–563 (2001)
26. I. Benedetti, F. Barbe, Modelling polycrystalline materials: An overview of three-dimensional grain-scale mechanical models, J. Multi. Model. **5(1)**, 1350002 (2013)
27. C. N'Guyen, F. Barbe, N. Osipov, G. Cailletaud, B. Marini, C. Petry, Micromechanical local approach to brittle failure in bainite high resolution polycrystals: A short presentation, Comput. Mater. Sci. **64**, 62–65 (2012)
28. R. Lebensohn, M. Montagnat, P. Mansuy, P. Duval, J. Meysonnier, A. Phi-lip, Modeling viscoplastic behavior and heterogeneous intracrystalline deformation of columnar ice polycrystals, Acta Mat. **57(5)**, 1405–1415 (2009)
29. A. Musienko, G. Cailletaud, Simulation of inter- and transgranular crack propagation in polycrystalline aggregates due to stress corrosion cracking, Acta Mat. **57**, 3840–3855 (2009)
30. C. Bouchet, B. Tanguy, J. Besson, S. Bugat, Prediction of the effects of neutron irradiation on the Charpy ductile to brittle transition curve of an A508 pressure vessel steel, Comp. Mat. Sci. **32(3-4)**, 294–300 (2005)
31. D. Bacon, Y. Osetsky, Modelling dislocation-obstacle interactions in metals exposed to an irradiation environment, Mat. Sci. Eng. A **400**, 353–361 (2005)
32. D. Bacon, Y. Osetsky, The atomic-scale modeling of dislocation-obstacle interactions in irradiated metals, J. Min. Met. Mat. Soc. **59**, 40–45 (2007)
33. B. Marini, Fragilisation par irradiation des aciers faiblement alliées pour cuves de rep, 2006

Cite this article as: Can-Ngon Nguyen, Georges Cailletaud, Fabrice Barbe, Bernard Marini, Duy-Duan Nguyen, Huy-Thien Phan, Identification of crystal plasticity parameters for a non-irradiated and irradiated A508 bainite steel, Metall. Res. Technol. **118**, 204 (2021)